Can Ganymede's magnetopause help us probe its subsurface ocean?

N. Kaweeyanun[1], A. Masters[1]

[1]Department of Physics, Imperial College London, U.K.

Corresponding author: N. Kaweeyanun

Corresponding author email: nk2814@ic.ac.uk

Key Points

- Ganymede's upstream magnetopause produces the Chapman-Ferraro (C-F) magnetic field, whose structure varies at Jovian half-synodic period.
- The C-F magnetic field will diffuse into but not through Ganymede's subsurface ocean, inducing a secondary magnetic response.
- The ocean's inductive response has general magnitude ~1–10 nT, which should be measurable by the upcoming JUICE mission.
-

Abstract

Permanently magnetic Ganymede carves a distinct magnetosphere inside Jupiter's larger magnetic domain, confined by ambient Jovian plasma and magnetic field along the upstream magnetopause. As Ganymede traverses the Jovian plasma sheet, ambient magnetoplasma conditions vary at half-synodic period (5.27 hr), leading to same-period oscillation in the Chapman-Ferraro (C-F) magnetic field produced by the magnetopause. We assess the C-F magnetic field as a unique excitation source for Ganymede's subsurface ocean. The magnetopause field is shown to diffuse into but not through the ocean, causing magnetic induction provided the liquid layer thickness is $>$ ~30 km. Then using an analytical model, we calculate maximum variation of the C-F field and estimate ~1–10 nT inductive response from the ocean subjected to the magnetopause's movement, a range detectable by the JUpiter ICy moon Explorer (JUICE) spacecraft. Hence, Ganymede's magnetopause may become a viable tool for future induction-based study of the moon's subsurface ocean.

Plain Language Summary

Ganymede is the only Solar System moon to produce its own magnetic field. The moon hence carves out a magnetic bubble inside Jupiter's much larger one. This bubble is asymmetrical, compressed on one side by inflowing Jovian plasma like a rock in water. Upstream boundary between Ganymede's and Jupiter's magnetic fields is called the magnetopause, which also produces a magnetic field that varies at 5.27 hr period (Jovian half-synodic). Saltwater ocean inside Ganymede will experience this variation, and in response generate a magnetic field whose signal should be detectable by the JUpiter ICy moon Explorer (JUICE) spacecraft, which will orbit Ganymede in the 2030's. Understanding this ocean-magnetopause interaction can provide an additional tool

for determining the ocean's depth and conductivity, furthering our knowledge of the structure that may harbour and host life on this unique Solar System moon.

Key Words

Ganymede, subsurface ocean, magnetopause, magnetic induction, analytical modelling

1. Introduction

Born with a molten iron core, Ganymede is the only permanently magnetic Solar System satellite (Anderson et al., 1996; Gurnett et al., 1996; Kivelson et al., 1996; Schubert et al., 1996). The primary Ganymedean dipole magnetic field is ~ 7 times stronger than the ambient Jovian field, which affords the moon a distinct magnetosphere (Kivelson et al., 1997; Kivelson et al., 1998; Kivelson et al., 2002). Surrounded by heavy ion plasma at all times, magnetofluid motions inside Ganymede's magnetosphere follow a Dungey-like convection cycle, driven by frequent and dominant magnetic reconnection on the upstream magnetopause (Collinson et al., 2018; Kaweeyanun et al., 2020; Kaweeyanun et al., 2021).

Fundamental analytical assessment reveals that average reconnection rate, which is most sensitive to ambient Jovian magnetoplasma conditions near the magnetopause, varies with Ganymede's latitude inside Jupiter's plasma sheet (Kaweeyanun et al., 2020). As the moon travels through the sheet twice per one Jovian rotation (10.53 hr), ambient conditions oscillate at Jovian half-synodic period (5.27 hr). As the result, the Chapman-Ferraro (C-F) currents produced by the magnetopause should also oscillate at the same period.

These currents, through their associated C-F magnetic field, confines Ganymede's magnetosphere by removing and enhancing the internal Ganymedean field outside and inside the magnetopause respectively, resulting in upstream compression of the magnetic domain (Chapman & Ferraro, 1940). A half-synodic variable compression of the moon's magnetospheric field is significant given that Ganymede likely contains a conducting subsurface ocean, whose inductive responses introduce transience to the moon's internal field (Kivelson et al., 2002).

Since the initial proposal for the ocean's existence, its magnetic induction potential has been studied in response to Jupiter's synodic rotation period (10.53 hr) and Ganymede's orbital period (171.57 hr) (Seufert et al., 2011). Excitation effects from these two sources have been evaluated through a three-layer, finite-conductivity Ganymede model (Vance et al., 2021), yielding sets of isolines where the ocean's inductive responses are computed as functions its depth and conductivity.

Both synodic and orbital excitations arise solely from Jupiter's magnetic field variation. In contrast, half-synodic C-F magnetic excitation uniquely relies on existence of the upstream magnetopause and therefore Ganymede's permanent

magnetism. This magnetopause excitation is distinct from half-synodic second harmonic of Jupiter's rotation, which has also been considered as an additional source for ocean excitation (Vance et al., 2021). Identification of magnetopause excitation will introduce a potential new signal for inductive ocean probing, whose measurement is central to objectives of the upcoming JUpiter ICy moon Explorer (JUICE) mission (e.g., Grasset et al., 2013).

In this paper, we seek to establish excitation capacity of the C-F magnetic field first by characterising its diffusion into Ganymede's interior, then by modelling its maximum variation and estimating the ocean's magnetic response. Our analytical method allows an efficient and effective assessment under realistic boundary conditions. However, without a direct numerical simulation, generation of depth-conductivity isolines from magnetopause excitation is beyond the scope of this paper and a future avenue of research.

1. **Diffusion of Chapman-Ferraro magnetic field**

Figure 1 illustrates inward diffusion of the C-F magnetic field toward Ganymede's interior. The magnetopause field must first penetrate through the conducting ionosphere (Eviatar, Vasyliūnas et al., 2001) in order to reach the subsurface ocean, assuming the outer ice shell is electrically insulated. Then, since the secondary induced field opposes the excitation field and halts diffusion, the C-F signal must not penetrate through the ocean for induction effects to be significant.

Each of Ganymede's ionosphere and subsurface ocean is assumed to be a stationary fluid shell of thickness L with finite constant conductivity σ. In this case, diffusion depth and time of the C-F magnetic field follow (Saur et al., 2010)

$$\delta_{\text{diff}} = \sqrt{\frac{2}{\sigma\mu_0\omega}} \#(1)$$

$$T_{\text{diff}} = \sigma\mu_0 L^2 \#(2)$$

where δ_{diff} and T_{diff} are characteristic depth and time scales, $\mu_0 = 4\pi \times 10^{-7}$ H/m is the permeability of free space, and $\omega = \frac{2\pi}{T}$ is the angular frequency of Jovian half-synodic C-F magnetic field variation ($T = 5.27$ hr). Eq. 1 asserts greater penetrative power for longer-period excitation field, and diffusion depth expectedly approaches zero as fluid conductivity approaches infinity. For contextualised analysis, diffusion depth and time are normalized with respect to shell thickness and excitation period respectively. Effective penetration will occur if diffusion depth exceeds shell thickness and diffusion time stays below excitation period, or in logarithmic terms

$$\log\left(\frac{\delta_{\text{diff}}}{L}\right) > 0 \#(3)$$

$$\log\left(\frac{T_{\rm diff}}{T}\right) < 0 \#(4)$$

We first compute normalised diffusion depths and times for Ganymede's ionosphere, with shell thickness and conductivity considered as independent variables. Thickness of the ionosphere is currently not well constrained. As the result, an upper limit value of 400 km is chosen, even though a realistic value may be <50 km, to limit possibility of false positive penetration. The thickness variable range is thus defined between $L = 0-400$ km with 1 km resolution. The ionospheric conductivity is also highly uncertain. Galileo magnetometer measurements yielded *height-integrated* conductivity of $\sigma_h = \sigma L = 2$ S (Kivelson et al., 2004), while particle observations offered a much higher value of $\sigma_h = 100$ S (Eviatar, Vasyliūnas, et al., 2001). Since only two data points are available, we consider each conductivity value as a distinct case.

Figure 2 shows logarithms of normalised diffusion depths and times of the C-F magnetic field in Ganymede's ionosphere. Diffusion length (time) expectedly decreases (increases) with increasing both ionospheric thickness and conductivity, indicating less successful penetration. However, even for the thickest and most conducting ionosphere, normalised diffusion depth (time) always remains above (below) 1 by at least one order of magnitude – comfortably satisfying Eq. 3–4. Hence, the C-F magnetic field will traverse through Ganymede's ionosphere with ease.

Next, we define viable ranges for thickness and conductivity of Ganymede's subsurface ocean. Like the ionosphere, large uncertainty remains regarding thickness of the liquid layer, which is either sandwiched thinly between two thick ice shells, or completely extended from the outer ice shell down to the silicate mantle (Kivelson et al., 2002). The ocean may be as thick as 700 km based on Galileo observations (Schubert et al., 1996; Stevenson, 1996; McKinnon, 1997), therefore this value is chosen as the upper limit of our thickness range ($L = 0 - 700$ km, 1 km resolution). The ocean conductivity, meanwhile, is not accessible without further in-situ observations. Hence, following the procedure in Kivelson et al., (2002), the Ganymedean ocean is assumed conductivity of Earth's i.e., $\sigma = 3-6$ S/m at 0.01 S/m resolution (Zheng et al., 2018). Note that these values are not height-integrated conductivities, and their high resolution reflect detailed sampling of the Earth's ocean rather than present knowledge of Ganymede's saltwater.

Consequently, Figure 3 displays logarithms of normalised diffusion depths and times of the C-F magnetic field in Ganymede's subsurface ocean. The diffusion parameters are shown as colour contours of ocean thickness and conductivity, with the white regions indicating where normalised diffusion depths (times) are above (below) 1. Minimum thickness for non-penetration and untimely diffusions are $30-40$ km and $60-70$ km respectively, differing because the diffusion parameters are computed separately. Here we take the lower threshold as the effective barrier to penetration. A more conducting ocean will reduce diffusive

ability of the C-F magnetic field, although the difference is not as significant as increasing ocean thickness.

Since Ganymede's subsurface ocean thickness is uncertain, it cannot be said definitely whether magnetopause-excited induction will occur. However, ocean thickness of $30-40$ km is highly possible given the scale of Ganymede's cross section, and a slightly thinner liquid layer would still result in significant attenuation of the C-F magnetic field. Therefore, on balance of probability, non-negligible inductive response should be expected at Jovian half-synodic period. In the next section, we seek to estimate the magnitude of this response, starting from analytical modelling of the C-F magnetic field and then estimating its maximum variation.

1. **Estimation of subsurface ocean's inductive response through analytical modelling of the C-F magnetic field**

To capture the C-F magnetic field, magnetopause current densities for Ganymede can be computed following (Glassmeier, Grosser et al., 2007; Glassmeier, Auster et al., 2007)

$$\mathbf{j}_{\mathrm{CF}} = -\frac{1}{\mu_0}\left(\mathrm{B}\times\mathbf{N}\right)\#(5)$$

where $\mathbf{j_{CF}}$ is per-length current density vector, $\mathbf{B}=\mathbf{B_J}-\mathbf{B_G}$ is cross-boundary difference between Jovian and Ganymedean magnetic vectors, and $\mathbf{N}$ is upstream-ward local magnetopause unit normal vector. The C-F current then follows

$$I_{\mathrm{CF}} = \int \mathbf{j}_{\mathrm{CF}} \bullet d\mathbf{l} \;\sim\; j_{\mathrm{CF}}\pi R_{\mathrm{MP}}\#(6)$$

where d$\mathbf{l}$ is a line element along an arbitrarily chosen path. Following Glassmeier, Grosser et al., (2007), we estimate the C-F current path as a semi-circular arc with a constant representative current density magnitude ($\mathrm{j_{CF}}$) calculated at the subflow point, where the magnetopause standoff distance ($\mathrm{R_{MP}}$) is measured. The associated C-F magnetic field is then parallel/antiparallel to Ganymede's rotation axis with magnitude

$$B_{\mathrm{CF}} = \frac{\mu_0 I_{\mathrm{CF}}}{2\pi} C\left(R_{\mathrm{MP}}, r\right)\#(7)$$

which is effectively Ampère's law with an inverse distance function

$$C\left(R_{\mathrm{MP}}, r\right) = \frac{1}{R_{\mathrm{MP}}+r}\left[K\left(\frac{r}{R_{\mathrm{MP}}}\right) + \left(\frac{R_{\mathrm{MP}}+r}{R_{\mathrm{MP}}-r}\right)E\left(\frac{r}{R_{\mathrm{MP}}}\right)\right]\#(8)$$

where r is the radial distance from Ganymede's centre at which the C-F magnetic field is measured. $K\left(\frac{r}{R_{\mathrm{MP}}}\right)$ and $E\left(\frac{r}{R_{\mathrm{MP}}}\right)$ are complete elliptic integrals of first and second kinds respectively. The C-F magnetic field strength in Eq. 7

decreases with distance from the magnetopause current sheet i.e., $r \to 0$, but problematically approaches infinity as $r \to R_{\mathrm{MP}}$ which is not the case in reality. The asymptotic fault arises from the 'thin-wire' assumption used to approximate the magnetopause current. Since C($\mathrm{R_{MP}}$, r) only spikes once r is considerably close to $\mathrm{R_{MP}}$, Eq. 7 is applicable if the C-F magnetic field is measured at sufficient distance from the boundary e.g., Ganymede's surface.

In this paper, Ganymede's magnetopause is parametrised following Kaweeyanun et al., (2020, 2021), whose equations are modified from original cylindrical description (Kivelson et al., 1998) for fixed Ganymede-centred Cartesian coordinate system (GphiO) where X is parallel to Jovian plasma inflow, Y points from Ganymede to Jupiter, and Z is parallel to Jupiter's (and approximately Ganymede's) rotation axis. The analytical model takes as inputs steady-state ambient Jovian magnetoplasma parameters, whose values are dictated by Jupiter's System III east longitude (λ_{III}) following

$$\rho_{J,0} = \left(\rho_{J,0}\right)_{\lambda_{\mathrm{III}}=248^{\circ}} \exp\left(\tfrac{-d}{H}\right)^{2} \#(9)$$

$$P_{J,0} = \left(P_{J,0}\right)_{\lambda_{\mathrm{III}}=248^{\circ}} \exp\left(\tfrac{-d}{H}\right)^{2} \#(10)$$

$$B_{J,0} = \left|35 \sin\left(\lambda_{\mathrm{III}} - 248^{\circ}\right)\right| + \left(B_{J,0}\right)_{\lambda_{\mathrm{III}}=248^{\circ}} \#(11)$$

where $\rho_{J,0}$ (amu/cm^3), $\mathrm{P_{J,0}}$ (nPa), and $\mathrm{B_{J,0}}$ (nT) are ambient Jovian plasma mass density, plasma (thermal and energetic combined) pressure, and magnetic field strength. Plasma density and pressure decrease, while magnetic field strength increases, with Ganymede's distance from centre of the Jovian plasma sheet ($\lambda_{\mathrm{III}} = 248^{\circ}$ in Eq. 9-12, but also $\lambda_{\mathrm{III}} = 68^{\circ}$) expressed by

$$d = (15\ R_J) \sin(6.3^{\circ}) \sin\left(\lambda_{\mathrm{III}} - 248^{\circ}\right) \#(12)$$

and $H = \frac{1.62}{\sqrt{ln2}}$ is chosen as the plasma sheet's scale height. The ambient Jovian magnetic field is assumed to have negligible inflow-aligned X component, and its Y-Z components (in nT) are distributed by (Jia et al., 2008; Kaweeyanun et al., 2020)

$$B_{J,0,y} = -84 \sin\left(\lambda_{\mathrm{III}} - 248^{\circ}\right) \#(13)$$

$$B_{J,0,z} = 3 \cos\left(\lambda_{\mathrm{III}} - 248^{\circ}\right) - 79 \#(14)$$

resulting in a field that deviates maximally $\approx 45^{\circ}$ from the negative Z-axis when Ganymede is at its highest ($\lambda_{\mathrm{III}} = 158^{\circ}$) and lowest ($\lambda_{\mathrm{III}} = 338^{\circ}$) latitude in

the Jovian plasma sheet. Compressions of ambient Jovian plasma and magnetic field vectors near the magnetopause are described in Kaweeyanun et al., (2020) with preservation of the ambient field direction. By fixing the magnetopause location, and conserving total Jovian (plasma, magnetic, and dynamic ram) pressure before and after near-boundary compression, Ganymede's magnetic field strength and direction inside the boundary can then be estimated assuming negligible pressure from cold Ganymedean plasmas (Kaweeyanun et al., 2020).

Using the descriptions above, cross-magnetopause magnetic field vector difference can be calculated at the subflow point, leading to the C-F magnetic field through Eq. 5–7. We set a fixed initial standoff distance $R_{\rm MP} = 1.65$ $\rm R_G$ and a measurement point $r = 1.0$ $\rm R_G$ on Ganymede's equatorial surface. Figure 4 shows variation of the C-F magnetic field as function of the Jovian System III east longitude, which is defined between $0^\circ - 360^\circ$ at 1° resolution – corresponding to one Jovian synodic period. Two oscillation periods are seen in the figure, indicating half-synodic oscillation of the C-F field consistent with expectation. Notably, the magnetopause field strength rapidly increases as Ganymede departs from the plasma sheet's centre ($\lambda_{\rm III} = 68^\circ,\ 248^\circ$), before declining beyond $|\Delta\lambda_{\rm III}| < \sim 20^\circ$ on either side of the central longitudes.

Non-monotony of the C-F magnetic field with respect to Ganymede's latitude in the plasma sheet arises due to similar variation in the Ganymedean magnetic field, which in this analytical model depends on the effective acting pressure – i.e., sum of plasma, magnetic, and boundary-orthogonal dynamic pressure – on the magnetopause. When Ganymede leaves the plasma sheet's centre ($\lambda_{\rm III} = 68^\circ,\ 248^\circ$), the Jovian magnetic pressure increases as $\rm B_{J,0}$ departs from local minima, but the other two pressures decrease due to reducing plasma mass density. Competition between these two trends manifest in the acting pressure, where magnetic pressure is dominant within $|\Delta\lambda_{\rm III}| <\sim 20^\circ$ the central longitudes and combined plasma-dynamic pressure is dominant elsewhere.

In Figure 4, maximum change in the C-F magnetic field strength is $\Delta B_{\rm CF} = -18.6$ nT between $\lambda_{\rm III} = 268^\circ$ and $\lambda_{\rm III} = 334^\circ$. Field values at two different longitudes can be directly subtracted as the C-F magnetic field is purely in Z-component of GphiO coordinates (0, 0, $\rm B_{CF}$). Importantly, the magnetopause is fixed at standoff distance $R_{\rm MP} = 1.65$ $\rm R_G$ during the maximum transition. This may not reflect reality where the boundary's movement is unclear, complicated by mixed influences of Jovian acting pressure and topology-changing interactions like magnetic reconnection (Kaweeyanun et al., 2020). Magnetopause motion impacts the standoff distance, which affect adjacent Jovian and/or Ganymedean magnetic fields and in turn the C-F field generated.

To evaluate effects of magnetopause movement, we again consider the maximum transition between $\lambda_{\rm III} = 268^\circ$ and $\lambda_{\rm III} = 334^\circ$. However, magnetopause standoff distance is allowed to vary between $R_{\rm MP} = 1.35{-}1.95$ $\rm R_G$ at 0.001 $\rm R_G$ resolution, which is approximately $\pm 18\%$ of the central $R_{\rm MP} = 1.65$ $\rm R_G$ derived from parameters in Kivelson et al., (1998). This range is not only significant, but also covers a discrepancy between the analytical model and numerical simulations,

in which Ganymede's standoff distance may extend as far as $R_{\rm MP} \sim 2$ $R_{\rm G}$ (Jia et al., 2008; Jia et al., 2009; Olsen et al., 2010). Changing the analytical model's standoff distance slightly alters the magnetopause's curvature, but this does not impact our results since representative C-F current density is taken at the subflow point.

Figure 5 shows the C-F magnetic field variation at Ganymede's surface between $\lambda_{\rm III} = 268^\circ$ and $\lambda_{\rm III} = 334^\circ$, accounting for potential magnetopause movements during the transition. Positive (negative) $\Delta R_{\rm MP}$ indicates outward (inward) motion from $R_{\rm MP} = 1.65$ $R_{\rm G}$. Outward boundary movement weakens the C-F magnetic field at Ganymede's surface and $\Delta B_{\rm CF}$ trends negatively. Conversely, inward movement increases the C-F field strength and $\Delta B_{\rm CF}$ trends positively. The y-intercept is $\Delta B_{\rm CF} = -18.6$ nT consistent with Figure 4. Meanwhile, the x-intercept is $\Delta R_{\rm MP} = -0.14$ $R_{\rm G}$, indicating that a slight inward magnetopause movement is required to negate change in the C-F magnetic field for this specific Ganymedean transition.

Given the precise values required, magnetopause motions cannot plausibly oppose C-F field variations exactly at all times, therefore excitation of Ganymede's subsurface ocean will occur. Magnitudes of $\Delta B_{\rm CF}$ in Figure 5 are upper limits of this excitation, from which we can estimate viable magnitudes of the inductive response. Take as example the y-intercept $\Delta B_{\rm CF} = -18.6$ nT. If the subsurface ocean is infinitely conducting, its inductive response will be dipolar with approximately half the exciting field's magnitude at Ganymede's surface (Saur et al., 2010), or $B^{\infty}_{\rm ind} \sim 9.3$ nT. Realistically, a finitely conducting ocean's response will be slightly smaller with the fractional difference of 0.84 (Kivelson et al., 2002), therefore $B_{\rm ind} \sim 7.8$ nT. Depending on to-be-constrained boundary movement, the oceanic response to magnetopause excitation is estimated to be of general order $B_{\rm ind} \sim 1 - 10$ nT at Ganymede's surface.

1. Discussion

Over the last two sections, we demonstrate that half-synodic variation of the C-F magnetic field will diffuse into Ganymede's subsurface ocean and produce an inductive response from the liquid layer. A signal of $B_{\rm ind} \sim 1 - 10$ nT magnitude should be visible to the magnetometer on the JUICE spacecraft, which will orbit Ganymede over extended periods in the 2030's (Grasset et al., 2013). Hence, the prediction of magnetopause excitation in this study should be confirmable by future in-situ observations.

Previously, magnetic contributions from Ganymede's current system have been studied under numerical magnetohydrodynamic simulations. Olsen et al., (2010) estimated current-associated magnetic field strength of ~ 50 nT at the magnetopause, based on conditions during the Galileo's G28 upstream flyby of the moon. Even though the flyby occurred significantly above and away from the moon's surface equator, the discrepancy to Figure 4 estimate of (~ 440 nT) is significant. The difference is partly attributed to the analytical model's closer magnetopause standoff distance (1.65 $R_{\rm G}$ vs. ~ 2 $R_{\rm G}$), and partly due to the

equatorial ring imperfect capture of the magnetopause currents. It must be noted that average C-F magnetic field at Ganymede's surface is $\sim 60\%$ of the moon's dipole moment (719 nT per Kivelson et al., 2002), which is roughly the same as results from similar-sized Mercury (58% per Grosser et al., 2004; Saur et al., 2010).

Improving constraint on Ganymede's magnetopause shape and movements, either through numerical simulations or early sample of JUICE's upcoming flybys/orbits, will narrow the expected range of the inductive response and offer potential insights its shape. This should allow magnetopause induction to be extracted from JUICE's future data and separated from responses to other excitations that may share similar periods (e.g., second harmonic of Jupiter's rotation).

In the meantime, the C-F magnetic field must be developed into a useful signal for probing Ganymede's subsurface ocean. The process will require computation of the magnetopause field's depth-conductivity response isolines, likely involving an induction numerical scheme (e.g., Vance et al., 2021) that includes three-dimensional characterisation of the C-F magnetic field. Once this is achieved, the magnetopause will be integrated into magnetic sounding of Ganymede's subsurface ocean, solidifying an important link that has been discovered in our analysis.

1. Conclusion

When Galileo made its flybys of Ganymede, the spacecraft discovered not only evidence of the moon's permanent internal magnetic field, but also support for existence of a subsurface ocean (Kivelson et al., 1996; Kivelson et al., 2002). Inductive response from the ocean has been studied at Jovian synodic (10.53 hr) and Ganymedean orbital (171.57 hr) periods, both in relation to Jupiter's magnetic field variation (Vance et al., 2021). In this paper, we predict that the Chapman-Ferraro (C-F) magnetic field, produced by Ganymede's unique upstream magnetopause and varying at Jovian half-synodic period (5.27 hr), is also a viable source of excitation for the subsurface ocean.

Computation of normalised diffusion depths and times show that the C-F magnetic field will comfortably penetrate Ganymede's conducting ionosphere, before being stopped in the ocean provided the liquid layer exceeds $30-40$ km in thickness, which is likely given current knowledge of Ganymede's interior. We model the C-F magnetic field using an equatorial current arc approximation (Glassmeier, Grosser et al., 2007; Glassmeier, Auster et al., 2007) and show that at maximum variation, the magnetopause will induce response of general magnitude $\sim 1-10$ nT from the subsurface ocean, which should be detectable by the upcoming JUICE spacecraft.

These findings establish the magnetopause as a potential tool for induction probing of the subsurface ocean, whose understanding remains limited despite its importance to JUICE's objectives. Although further research development is necessary for more precise and applicable predictions, magnetopause-produced

magnetic induction at Ganymede is a signal worthy of investigation in the immediate future.

Acknowledgments

N. Kaweeyanun is supported by a Royal Society PhD Studentship. A. Masters is supported by a Royal Society University Research Fellowship**.** Derived data in Figures 2–5 is available in the Imperial College High Performance Computing Service Data Repository (Kaweeyanun, 2022).

Reference

Anderson, J.D., Lau, E.L., Sjogren, W.L., Schubert, G., Moore, W.B. (1996). Gravitational constraints on the internal structure of Ganymede. *Nature*, 384 (6609), 541-543. https://doi.org/10.1038/384541a0

Chapman, S. & Ferraro, V.C.A. (1940). The Theory of the First Phase of a Geomagnetic Storm. *Terrestrial Magnetism and Atmospheric Electricity*, 45 (3), 245-268. http://doi.org/10.1029/TE045i003p00245

Collinson, G., Paterson, W.R., Bard, C., Dorelli, J., Glocer, A., Sarantos, M., Wilson, R.J. (2018) New Results from *Galileo's* First Flyby of Ganymede: Reconnection-Driven Flows at the Low-Latitude Magnetopause Boundary, Crossing the Cusp, and Icy Ionospheric Escape. *Geophys. Res. Lett.*, 45 (8), 3382-3392. https://doi.org/10.1002/2017GL075487

Eviatar, A., Vasyliūnas, V.M., Gurnett, D.A. (2001). The ionosphere of Ganymede. *Planet. Space Sci.*, 49 (3-4), 327-336. https://doi.org/10.1016/S0032-0633(00)00154-9

Glassmeier, K.-H., Auster, H.-U., Motschmann, U. (2007). A feedback dynamo generating Mercury's magnetic field. *Geophys. Res. Lett.*, 34 (22), L22201. https://doi.org/10.1029/2007GL031662

Glassmeier, K.-H., Grosser, J., Auster, U., Constantinescu, D., Narita, Y., Stellmach, S. (2007). Electromagnetic Induction Effects and Dynamo Action in the Hermean System. *Space Sci. Rev.*, 132 (2), 511-527. https://doi.org/10.1007/s11214-007-9244-9

Gurnett, D.A., Kurth, W.S., Roux, A., Bolton, S.J., Kennel, C.F. (1996). Evidence for a magnetosphere of Ganymede from plasma-wave observations by the Galileo spacecraft. *Nature*, 384 (6609), 535-537. http://doi.org/10.1038/384535a0

Grasset, O., Dougherty, M.K., Coustenis, A., Bunce, E.J., Erd, C., Titov, D., Blanc, M., Coates, A., Drossart, P., Fletcher, L.N., Hussmann, H., Jaumann, R., Krupp, N., Lebreton, J.-P., Prieto-Ballesteros, O., Tortora, P., Tosi, F., Van Hoolst, T. (2013). JUpiter ICy moon Explorer (JUICE): An ESA mission to orbit Ganymede and characterise the Jupiter system. *Planet. Space Sci.*, 78, 1-21. https://doi.org/10.1016/j.pss.2012.12.002

Grosser, J., Glassmeier, K.-H., Stadelmann, A. (2004). Induced magnetic field effects at planet Mercury. *Planet. Space Sci.,* 52 (14), 1251-1260. https://doi.org/10.1016/j.pss.2004.08.005

Jia, X., Walker, R.J., Kivelson, M.G., Khurana, K.K., Linker, J.A. (2008). Three-dimensional MHD simulations of Ganymede's magnetosphere. *J. Geophys. Res.*, 113 (A6), A06212. https://doi.org/10.1029/2007JA012748

Jia, X., Walker, R.J., Kivelson, M.G., Khurana, K.K., Linker, J.A. (2009). Properties of Ganymede's magnetosphere inferred from improved three-dimensional MHD simulations. *J. Geophys. Res.*, 114 (A9), A09209. https://doi.org/10.1029/2009JA014375

Kaweeyanun, N. (2022). *Can Ganymede's magnetopause help us probe its subsurface ocean?* Imperial College London Research Data Depository. https://doi.org/10.14469/hpc/11104. [Dataset]

Kaweeyanun, N., Masters., A., Jia, X. (2020). Favorable Conditions for Magnetic Reconnection at Ganymede's Upstream Magnetopause. *Geophys. Res. Lett.*, 47 (6), e2019GL086228. https://doi.org/10.1029/2019GL086228

Kaweeyanun, N., Masters., A., Jia, X. (2021). Analytical Assessment of Kelvin-Helmholtz Instability Growth at Ganymede's Upstream Magnetopause. *J. Geophys. Res. Space Phys.*, 126 (8), e2021JA029338. https://doi.org/10.1029/2021JA029338

Kivelson, M.G., Bagenal, F., Kurth, W.S., Neubauer, F.M., Paranicas, C., Saur, J. (2004). Magnetospheric Interactions with Satellites. In *Jupiter: The Planet, Satellites, and Magnetosphere.* F. Bagenal, T.E. Dowling, W.B. McKinnon (ed.). Cambridge, United Kingdom: Cambridge University Press, 513-536. Bibcode: 2004jpsm.book..513K

Kivelson, M.G., Khurana, K.K., Coroniti, F.V., Joy, S., Russell, C.T., Walker, R.J., Warnecke, J., Bennett, L., Polanskey, C. (1997). The magnetic field and magnetosphere of Ganymede. *Geophys. Res. Lett.*, 24 (17), 2155-2158. https://doi.org/10.1029/97GL02201

Kivelson, M.G., Khurana, K.K., Russell, C.T., Walker, R.J., Warnecke, J., Coroniti, F.V., Polanskey, C., Southwood, D.J., Schubert, G. (1996). Discovery of Ganymede's magnetic field by the Galileo spacecraft. *Nature*, 384 (6609), 537-541. http://doi.org/10.1038/384537a0

Kivelson, M.G., Khurana, K.K., Volwerk, M. (2002). The Permanent and Induced Magnetic Moments of Ganymede. *Icarus*, 157 (2), 507-522. https://doi.org/10.1006/icar.2002.6834

Kivelson, M.G., Warnecke, J., Bennett, L., Joy, S., Khurana, K.K., Linker, J.A., Russell, C.T., Walker, R.J., Polanskey, C. (1998). Ganymede's magnetosphere: Magnetometer overview. *J. Geophys. Res.*, 103 (E9), 19,963-19,972. https://doi.org/10.1029/98JE00227

McKinnon, W.B. (1997). Galileo at Jupiter – meetings with remarkable moons. *Nature*, 390 (6655), 23-26. http://doi.org/10.1038/36222

Olsen, N., Glassmeier, K.-H., Jia, X. (2010). Separation of the Magnetic Field into External and Internal Parts. *Space Sci. Rev.*, 152 (1), 135-157. https://doi.org/10.1007/s11214-009-9563-0

Saur, J., Neubauer, F.M., Glassmeier, K.-H. (2010). Induced Magnetic Fields in Solar System Bodies. *Space Sci. Rev.*, 152 (1), 391-421. http://doi.org/10.1007/s11214-009-9581-y

Schubert, G., Zhang, K., Kivelson, M.G., Anderson, J.D. (1996). The magnetic field and internal structure of Ganymede. *Nature*, 384 (6609), 544-545. http://doi.org/10.1038/384544a0

Seufert, M., Saur, J., Neubauer, F.M. (2011). Multi-frequency electromagnetic sounding of the Galilean moons. *Icarus*, 214 (2), 477-494. https://doi.org/10.1016/j.icarus.2011.03.017

Stevenson, D.J. (1996). When Galileo met Ganymede. *Nature*, 384 (6609), 511-512. http://doi.org/10.1038/384511a0

Vance, S.D., Styczinski, M.J., Bills, B.G., Cochrane, C.J., Soderlund, K.M., Gómez-Pérez, N., Paty, C. (2021). Magnetic Induction Responses of Jupiter's Ocean Moons Including Effects From Adiabatic Convection. *J. Geophys. Res. Planets*, 126 (2), e2020JE006418. https://doi.org/10.1029/2020JE006418

Zheng, Z., Fu, Y., Liu, K., Xiao, R., Wang, X., Shi, H. (2018). Three-stage vertical distribution of seawater conductivity. *Scientific Reports*, 8 (1), 9916. https://doi.org/10.1038/s41598-018-27931-y

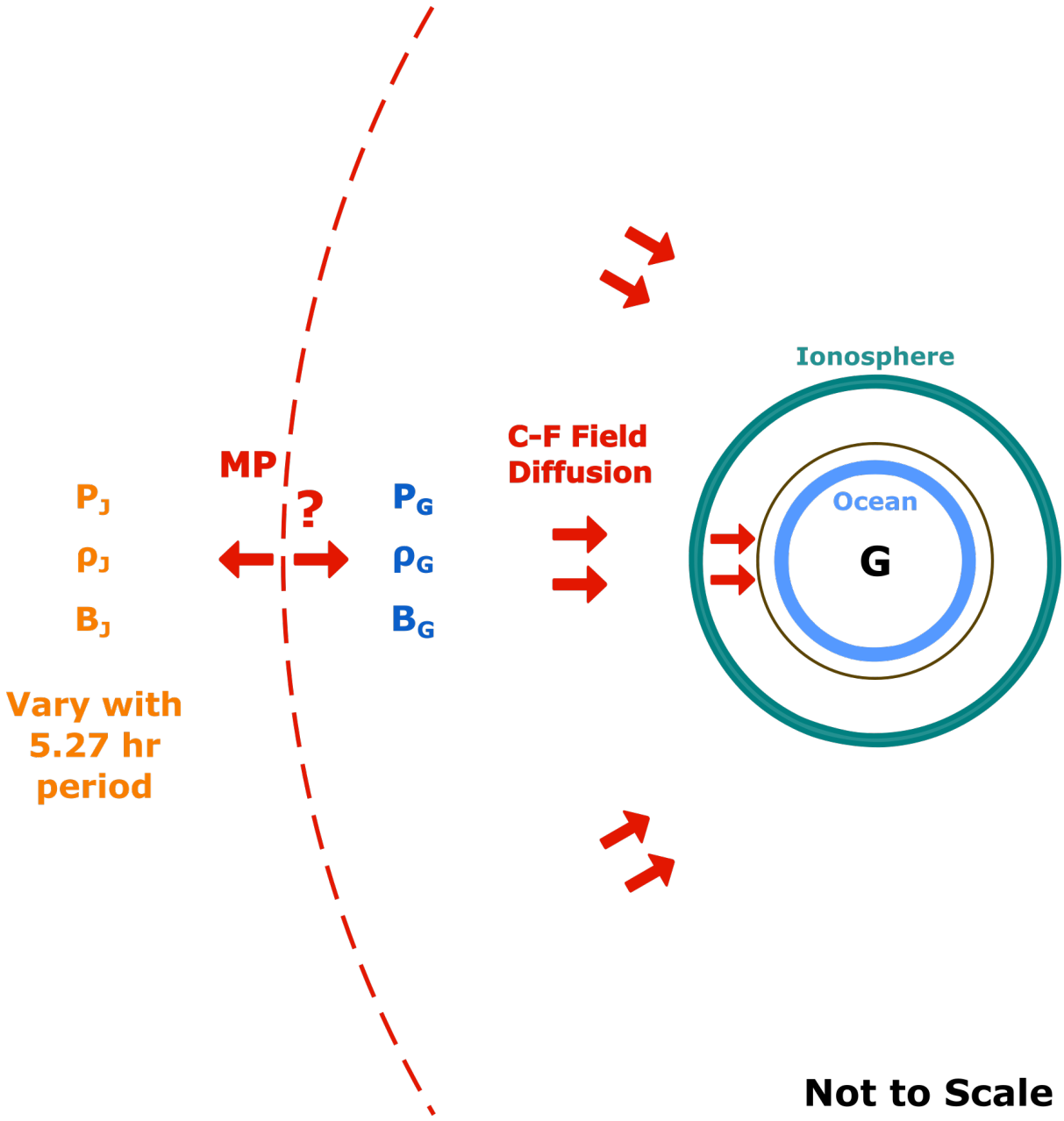

Figure 1: Schematic diagram for diffusion of half-synodic Chapman-Ferraro (C-F) magnetic field from Ganymede's magnetopause through its conducting ionosphere, and later into its subsurface ocean.

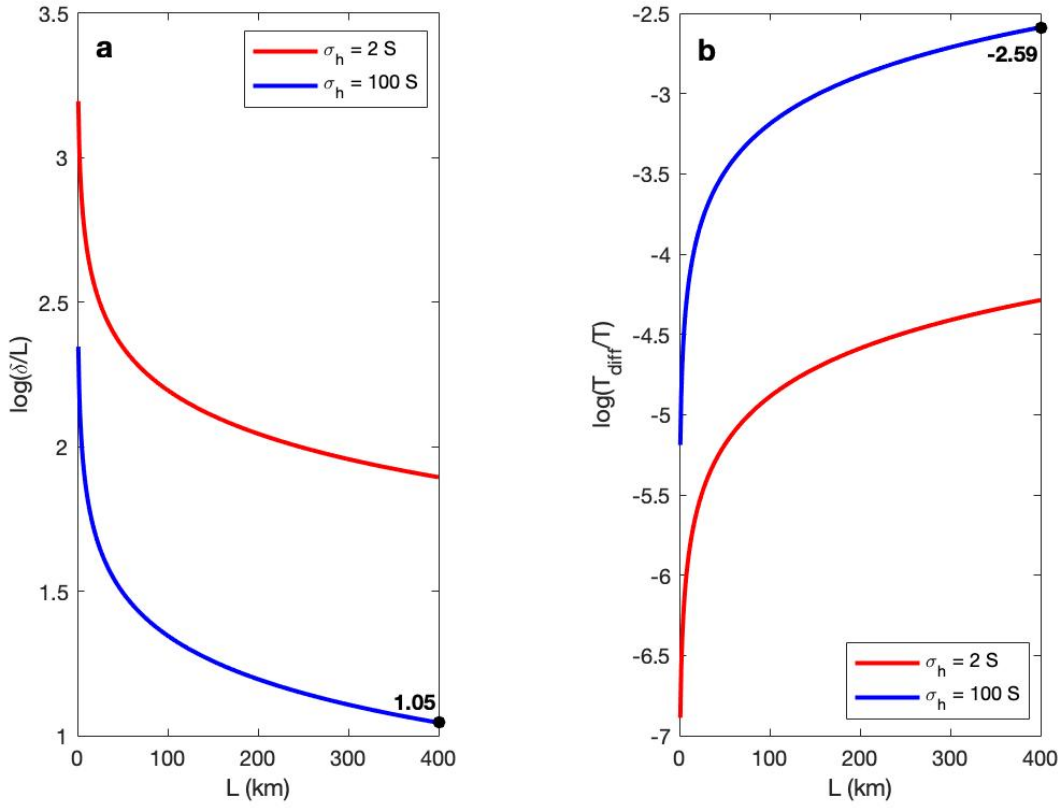

Figure 2: Normalised diffusion depth (a) and time (b) of the C-F magnetic field through Ganymede's ionosphere of varying thicknesses for low (red) and high (blue) height-integrated ionospheric conductivities.

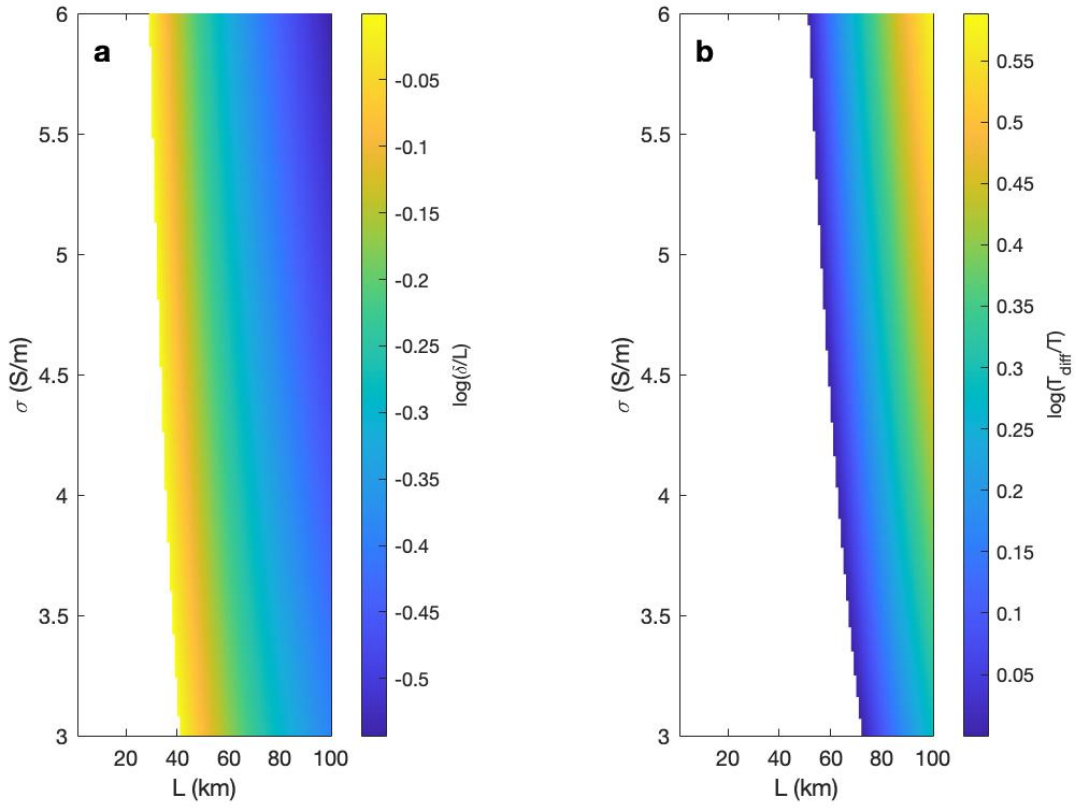

Figure 3: Normalised diffusion depth (a) and time (b) as contour plots with respect to Ganymede's subsurface ocean thickness and conductivity. In the white region, complete diffusive penetration occurs. Ocean thickness is displayed only up to 100 km for clarity of subplots.

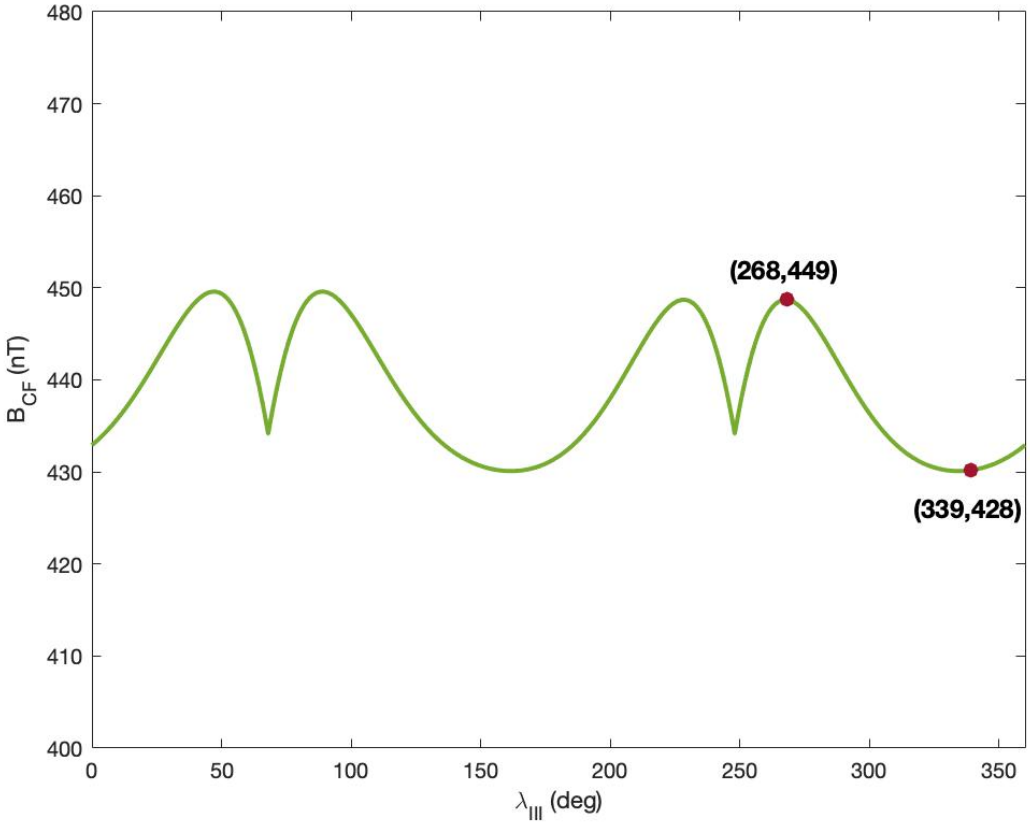

Figure 4: The C-F magnetic field magnitude at Ganymede's equatorial surface, estimated from magnetopause current at the subflow point, with respect to System-III Jovian east longitude over one Jovian synodic period. Maximum and minimum B_{CF} are found at $\lambda_{III} = 268^{\circ}$ and $\lambda_{III} = 339^{\circ}$ respectively (maroon dots).

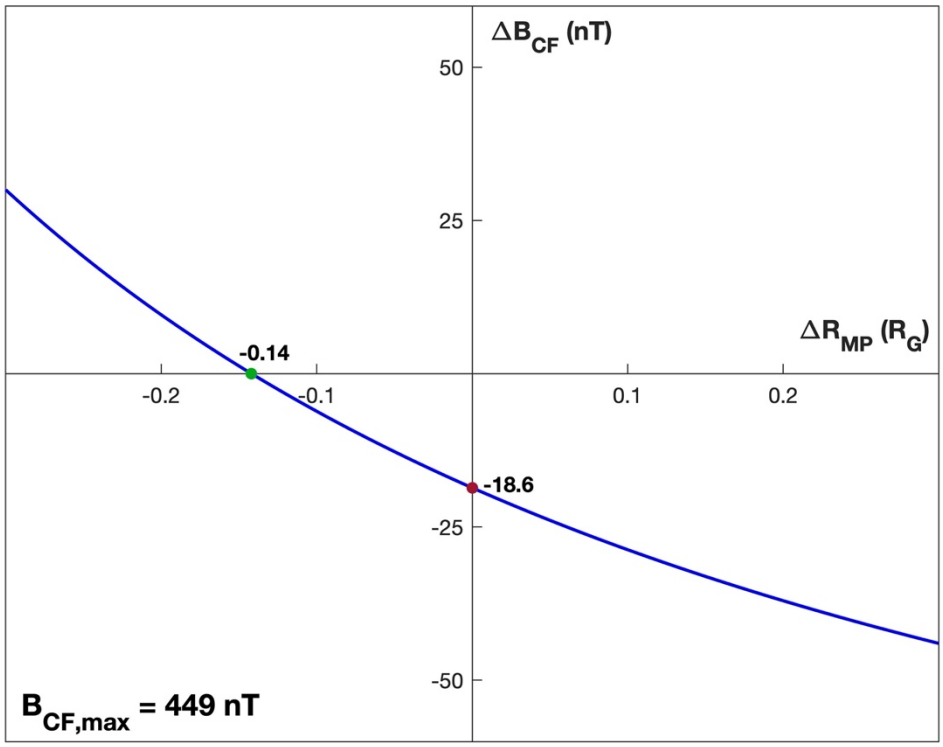

Figure 5: Change in C-F magnetic field strength as function of magnetopause location for 'maximum transition' $\lambda_{\mathrm{III}} = 268^{\circ}$ to $\lambda_{\mathrm{III}} = 334^{\circ}$, relative to central $B_{CF,max} = 449$ nT at $R_{\mathrm{MP}} = 1.65$ $\mathrm{R_G}$. Positive (negative) R_{MP} corresponds to outward (inward) boundary movement. X and Y intercepts of the curve is marked in green and red respectively.